

RSC Advances



This is an *Accepted Manuscript*, which has been through the Royal Society of Chemistry peer review process and has been accepted for publication.

Accepted Manuscripts are published online shortly after acceptance, before technical editing, formatting and proof reading. Using this free service, authors can make their results available to the community, in citable form, before we publish the edited article. This *Accepted Manuscript* will be replaced by the edited, formatted and paginated article as soon as this is available.

You can find more information about *Accepted Manuscripts* in the [Information for Authors](#).

Please note that technical editing may introduce minor changes to the text and/or graphics, which may alter content. The journal's standard [Terms & Conditions](#) and the [Ethical guidelines](#) still apply. In no event shall the Royal Society of Chemistry be held responsible for any errors or omissions in this *Accepted Manuscript* or any consequences arising from the use of any information it contains.

ARTICLE

The evolution of GaN/sapphire interface with different nucleation layer thickness during two-step growth and its influence on the bulk GaN crystal quality

Cite this: DOI: 10.1039/x0xx00000x

Received 00th January 2012,
Accepted 00th January 2012

DOI: 10.1039/x0xx00000x
www.rsc.org/

Lin Shang,^{ab} Taiping Lu,^{ab} Guangmei Zhai,^{ab} Zhigang Jia,^{ab} Hua Zhang,^{ab} Shufang Ma,^{ab} Tianbao Li,^{ab} Jian Liang,^{ab} Xuguang Liu,^{ac} Bingshe Xu^{*ab}

The role of the nucleation layer thickness on the GaN crystal quality grown by metal organic chemical vapor deposition is explored. Surface morphologies of low-temperature GaN nucleation layer (NL) investigated by Atomic Force Microscopy shows the nuclei grains size increases with thickness increasing. After annealing, island-like morphologies of the low-temperature GaN NL are obtained. Increasing the NL thickness is beneficial for obtaining larger island size, however, the uniformity of the island size is deteriorated. The high-resolution X-ray diffraction analysis reveals that bulk GaN crystal properties are closely connected with NL thickness, which can be well explained by the dislocation generation and propagation process in the GaN films. All the obtained results indicate that the NL thickness effectively controls the size and density of the islands and thus determines the crystal properties of GaN films.

1. Introduction

Nitride semiconductors are presently one of the most promising materials for optoelectronic devices operating in the ultraviolet-to-green wavelength regions.¹ The surface morphology and crystalline quality of GaN films are the key factors for the realization of high performance GaN based devices. GaN is usually heteroepitaxially grown on sapphire because of its low cost, superior material quality and availability in large-sized wafers. Owing to the large lattice mismatch between GaN and sapphire, the low-temperature GaN nucleation layer (NL) growth and annealing are necessary processes to obtain high quality bulk GaN.² The optimization of NL plays the most important role in growth of high quality GaN and reduction of the threading dislocation (TD). TDs are known to play detrimental effects on device performance, such

as non-radiative recombination centers³, and reduce the lifetime of devices by acting as diffusion channels between the electrodes.⁴ The optimization of this important layer has been widely reported in literature.⁵⁻⁸ Flat surface morphology of GaN film is good at obtaining multiple quantum well structure with abrupt interface. However, only little work has been carried out to microscopically investigate the evolution of GaN morphology during different growth stage such as NL, annealing, islands lateral overgrowth and coalescence. After the annealing of NL, three-dimensional (3D) islands will form. The lateral growth of 3D islands will reduce the TD density in GaN film. So it is necessary to investigate the 3D islands evolution under different situation.

In this study, the physical mechanism of the effect of different nucleation thickness on crystal quality of bulk GaN epilayers is clarified. The surface morphology of the NL before and after annealing measured by atomic force microscopy (AFM) shows that thicker NL gives the larger nuclei island size. However, the uniformity of the island gets worse for thicker NL. Based on dislocation generation and propagation processes in films, the correlation between the NL thickness and bulk film crystal quality is proposed, which is further proved by high-resolution X-ray diffraction (HRXRD) results.

2. Experimental

¹ *a* Key Laboratory of Interface Science and Engineering in Advanced Materials Taiyuan University of Technology, Ministry of Education, Taiyuan, 030024, P.R.China. E-mail: xubs@tyut.edu.cn; Fax: +86 351 6010311; Tel: +86 351 6010311

^b Research Center of Advanced Materials Science and Technology, Taiyuan University of Technology, Taiyuan, 030024, P.R.China

^c college of Chemistry and Chemical Engineering, Taiyuan University of Technology, Taiyuan, 030024, P.R.China

The GaN films were grown on sapphire by 3×2” wafer metal organic chemical vapor deposition (MOCVD, Aixtron TS300) system. TMGa and NH₃ were used as precursors and H₂ as carrier gas. The sapphire was thermally cleaned at 1075°C under hydrogen for 6 min for the removal of possible impurities. The temperature was then reduced to 570°C and NH₃ flow was switched on to nitride the sapphire substrate for 360 s. Then at the same temperature, TMGa flow was switch on to grow GaN NL at 600 mbar and the growth times of three sample were 105, 180 and 315 s, corresponding to NL thickness 15, 25 and 45 nm, respectively. The substrate temperature was then ramped to the growth temperature of 1080°C with a ramping rate of 80°C/min and maintained at this temperature for 2 min. The process of temperature ramps and maintains is a decomposition-recrystallization process of NL. Then a 2-μm undoped GaN film was deposited with a growth rate 2.2 μm/h.

A semiconductor laser operating at a wavelength of 632.8 nm was used as in-situ monitoring tool to investigate the reflectance throughout the growth progress. The surface morphology during different stages was studied by AFM (SPA-300HV). AFM measurement was carried out at tapping model and the tip radius curvature is 10 nm. The crystal properties of bulk GaN epilayers were characterized by HRXRD (Bruke D8) with a 0.154178 nm Cu Kα rotating anode point source operating at 40 kV and 40 mA.

3. Result and discussion

It is known that in-situ optical reflectivity measurement is a powerful tool for monitoring material growth.¹⁰⁻¹² The reflectivity traces of three samples are shown in Fig 1. The growth process can be divided into four stages (1, 2, 3 and 4) corresponding to NL, annealing, lateral growth and two-dimensional (2D) growth stage, respectively. In the first stage, GaN NL is deposited at 570°C, leading to a higher reflectivity due to the larger refractive index than sapphire. The increased reflectivity, in stage 1, can provide the thickness of NL, which is estimated as 15nm, 25nm and 45nm, respectively. The reflectivity increases linearly with growth time and the 45 nm NL has the highest reflectivity. During the temperature ramping and stable in 1080°C corresponding to stage 2, the surface roughens and three-dimensional (3D) islands grow. Meanwhile the progress reduces the average thickness due to partially etching away under hydrogen. As a result, the reflectivity drops even below the value of the bare sapphire wafer. Generally, the reflectivity at the end of stage 2 is close to that of bare sapphire although the NL is not completely etched away, only a part of sapphire surface is covered with GaN islands. The early stage of un-doped GaN growth at 1080°C corresponding to stage 3 is the lateral growth and the coalescence of islands. At the beginning of this stage, the reflectivity drops close to zero, indicating a significant surface roughening. The stage 4, the reflectivity begins to oscillate and a smooth surface has been established. A stable reflectivity oscillation occurs in this stage as the thickness increases. It is obvious that the thicker the NL is, the longer the lateral growth time (stage 3) is. During stage 4, it can be seen that 15 nm-sample’s oscillation has the biggest peak-to-valley amplitudes of oscillation, 25 nm-sample smaller and 45 nm-sample smallest.

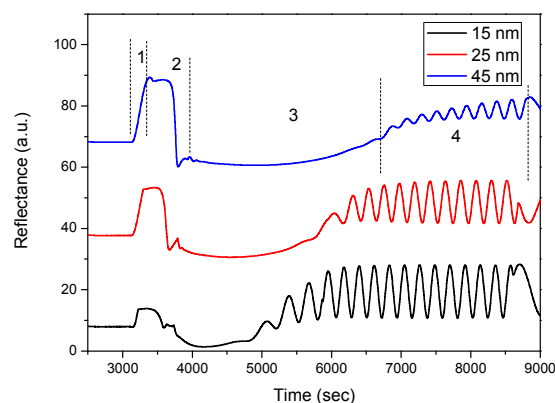


Fig 1 The reflectance recorded during the whole growth process of 15 nm-, 25 nm- and 45 nm-thick samples.

The samples grown at the end of different stages were analyzed by AFM. The AFM image at the end of stage 1, 2, 3 and 4 corresponds to Fig 2 (a) - (c), 2 (d) - (f), 5 and 6, respectively. The morphologies of three NLs before and after annealing are shown in Fig 2. Before annealing, the surface of all three samples is covered with dense grains, but their grain size increases from 15 nm-NL to 45 nm-NL samples, simultaneously leading to the decrease of the grain density. The average grain sizes of 15 nm-, 25 nm- and 45 nm-NLs are 80, 120 and 190 nm, respectively. The surface roughness σ in thin films deposition methodologies in which the film thickness h , is proportional to the time of deposition t , then, in the asymptotical limits,

$$\sigma(h) = ah^{\beta} \quad (1)$$

Where α and β are the roughness exponent and growth exponent. The value σ for each sample was calculated by averaging the values obtained by AFM images. The σ is 3.36, 4.15 and 5.35 nm for 15, 25 and 45 nm-NL, respectively. The roughness σ of NL as a function of the film thickness h in a log-log scale is shown in Fig 3. We fitted the experiment data in Fig 3 by equation (1) obtaining the growth exponent $\beta=0.41$ and roughness exponent $\alpha=1.05$. The values of β and α indicate that the deposition of NL on sapphire is a conservative deposition process, in agreement with the Siegert - Plischke (SP) equation¹³⁻¹⁵.

It has been reported that the GaN NL grown at such a low temperature is highly defective with mixed cubic and wurtzite phase and easy to decompose at high temperature.¹⁶ After annealing the morphologies of low-temperature GaN NLs are island-like (Figure 2 (d) - (f)). The nucleation islands (NIs) of 15 nm-NL have the highest density and smallest size; the islands of 45 nm-NL have lowest density and the largest size, but they are not uniform anymore. As marked by black circles in Fig 2 (f), some much smaller islands occur on the 45 nm-NL sample. As for 25 nm-NL, both its size and density are medium. The height distribution of islands are shown in Fig 4. Statistical measurements based on AFM images show that

most of the 15 nm-NIs have heights ranging from 30 to 70 nm, 25nm-NIs ranging from 160 to 200 nm. But for 45 nm-NIs, the height distribution ranges from 70 to 470 nm, among them many are small islands with size ranging from 70 to 170 nm. Among them, 25nm-NL's islands have the most uniform height.

The NL annealing is a decomposition-redeposition process proposed by Lorenz¹⁷ and Narayanan¹⁸ to account for the structural evolution of GaN NL during annealing in MOCVD. During annealing, some grains decompose and some grow up. Finally, the NL after annealing is island-like, as shown in Fig 2 (d) - (f). A film with fewer grains should tend to form larger islands spaced far apart and maintain a three-dimensional growth for a longer period of time. So in Fig 1, the sample with thicker NL has the longer lateral growth time. On the other hand, a film with more grains would form smaller islands that are spaced more closely and thus coalesce quickly. Because small islands coalesce for the 15 nm sample, the sapphire/GaN interface is smoother than the other samples, the peak-to-valley ratio of reflectivity fringes is higher because of the smoother interface. In the 45 nm sample, maybe the space is too long, Ga atoms react with NH₃ and redeposit on the bare sapphire surface to form some new and smaller islands. In the following epilayer growth, these islands act as nucleation sites and grow both vertically and laterally until they coalesce with each other. Some models are provided for secondary grain growth of other semiconductors which is similar with NL annealing. Theoretical analysis for grains growth under different stage including initial

grain structure, recrystallization process and grain growth have been development¹⁹⁻²¹.

Fig 5 is the AFM images of surface at the first period of periodic oscillation corresponding to the end of stage 3. At this point, the islands nearly coalesce with each other. Since the islands are somewhat misoriented relative to each other, the majority of edge-type TDs is generated at the coalescence boundaries.²² For 15 nm sample, the boundary area is large, which is caused by high density islands. As to 25 nm sample, the boundary area is less and the surface is flat. And for 45 nm sample, the surface is not flat, which is caused by different island size. So 15 nm sample tends to grow bulk GaN with many edge-type TDs. The 25 nm sample should grow a high quality GaN. As to 45 nm sample, the different height of surface is bad to its quality.

An AFM measurement was carried out in a 5 μm ×5 μm area to study the surface morphology of bulk GaN layer. As seen in Figure 6, the samples grown with 15 and 25 nm NL exhibit a smooth surface morphology with easily identified atomic steps. On the surface, there are also some dark spots which correspond to dislocations. The RMS roughness of 15 and 25 nm samples are 0.28 and 0.22 nm, respectively. Step terminations on a single crystal surface correspond to the intersection of a threading dislocation with the free surface.²³ The terminated steps and roughness of 25 nm sample are less than those of 15 nm sample. For 45 nm sample, some cracks and hillocks

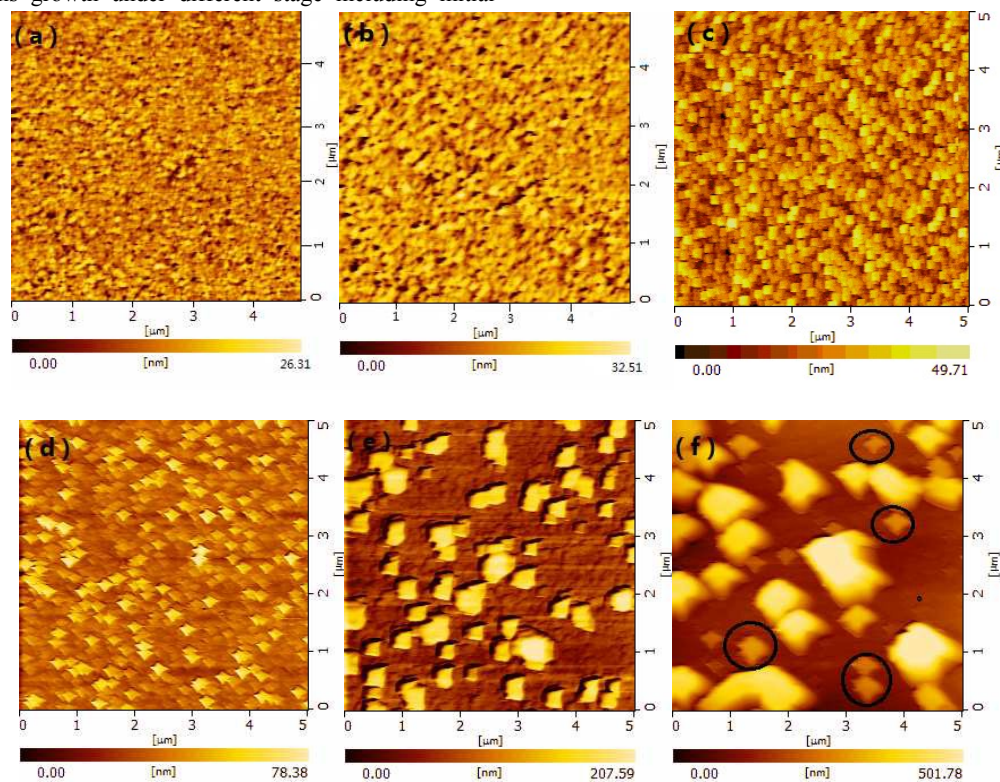


Fig 2 The AFM images (5×5 μm) for GaN NL before annealing : (a), (b), (c); and after annealing (d), (e), (f) with 15, 25 and 45 nm thickness

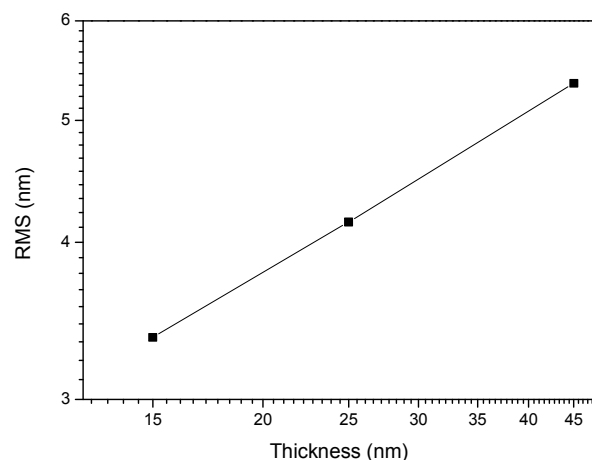


Fig 3 The roughness σ of NL as a function of the film thickness h in a log-log scale

can be observed and the steps are not flat. Its RMS roughness is 2.51 nm, much larger than others. The line profiles of the three sample are also shown in Figure 6. The terrace width of 15 nm sample is about 110 nm and the terrace height is about 0.5 nm with two atomic layer thickness. But the terrace is not uniform compared with 25 nm sample. The bad uniformity may come from the high surface stress induced by high dislocation density. The terrace width and height of 25 nm sample is about 90 nm and 0.5 nm, respectively and it is uniform. As to 45 nm sample, due to its bad morphology, the terrace width from 100 nm to 500 nm. In order to determine the dislocation density exactly, the chemical etching was carried out in a mixture H_2SO_4 and H_3PO_4 with a ratio of 1:3 at $240^\circ C$ for 5 min. Fig 7 shows the AFM images revealing etch pits on the GaN surface. These etch pits might have been produced by threading dislocations propagating to the top surface of GaN. Through measuring the etch pits density, the dislocation density can be obtained. The etch pits density of 15, 25 and 45 nm samples is 3.5×10^8 , 2×10^8 and $5 \times 10^8 cm^{-2}$, respectively. This result indicates the 25 nm sample has the lowest dislocation density, which agrees with the analysis before.

In order to explore the influence of different NL thickness on the crystal qualities of bulk GaN epilayers, the crystal qualities of bulk GaN are characterized by rocking curves of (002) and (102) planes in XRD measurement. The (002) plane scan centers at 17.4° at a scan rate of $0.005^\circ/s$ in the range from 15.4° to 19.4° and (102) plane centers at 24° at scan rate of $0.003^\circ/s$ in the range from 23.5° to 24.5° . The densities of the screw-type dislocations and the edge-type dislocations can be valued by the full width at half maximum (FWHM) of the ω -scan rocking curve of (002) and (102) planes, respectively.²⁴⁻²⁷ Fig 8 shows the FWHM of HRXRD ω -scan rocking curves as a function of the NL thickness. For 15 nm sample, the FWHMs of (002) and (102) are 312 and 466 arcsec, respectively. When the thickness of NL increases to 25 nm, the FWHMs of (002) and (102) decrease to 267 and 284 arcsec,

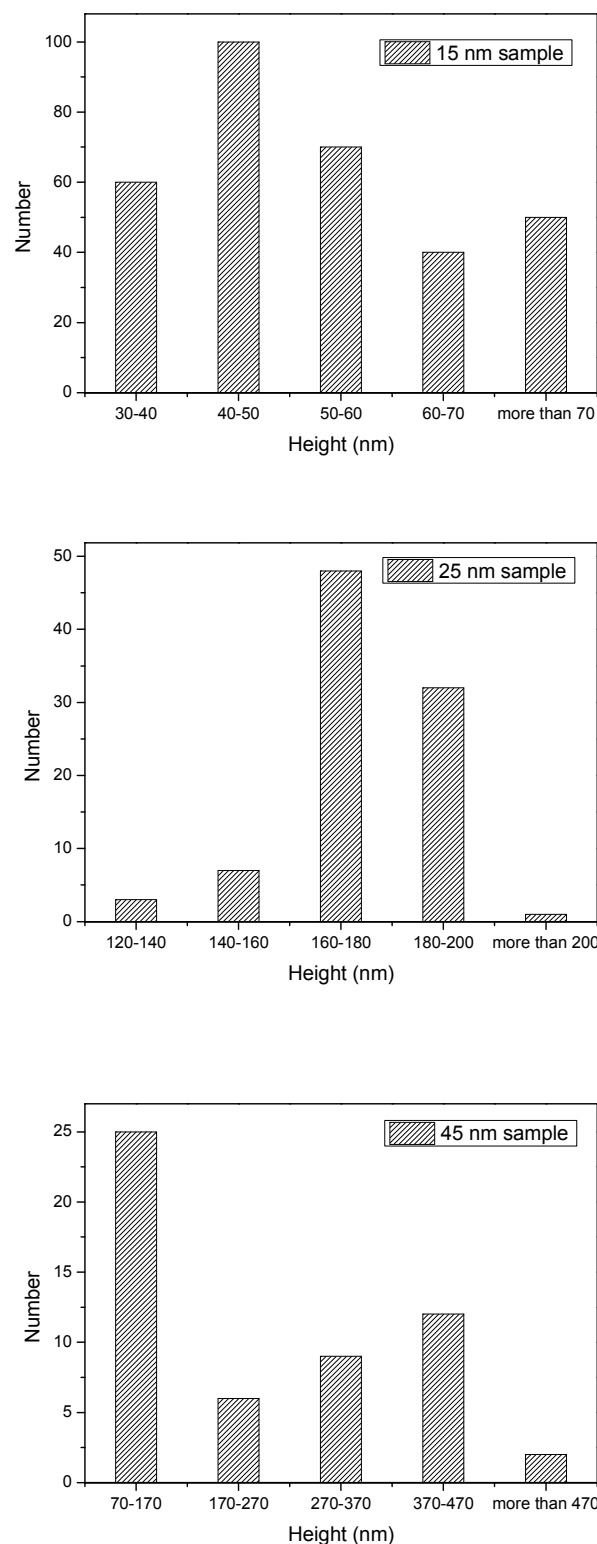


Fig 4 The height distribution of nucleation islands for 15, 25 and 45 nm NL after annealing

ARTICLE

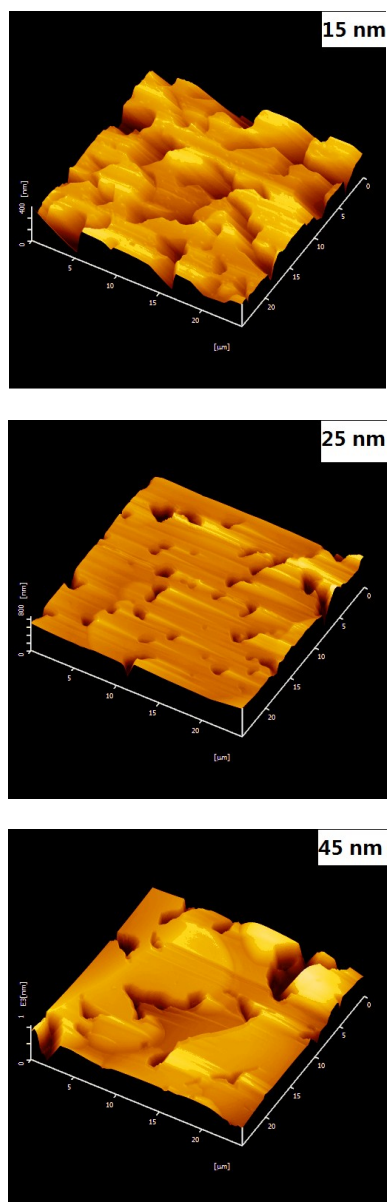


Fig 5 the AFM images (25×25 μm) of 3D to 2D surface with 15, 25 and 45 nm-NL thickness

respectively. However, with the further increase of NL thickness to 45 nm, the FWHMs of (002) and (102) increase to 327 and 339

arcsec instead of further decreasing. The dislocation density of edge and screw type can be estimated using the following equations:²⁸

$$D_{screw} = \frac{\beta_{(002)}^2}{9b_{screw}^2}, \quad D_{edge} = \frac{\beta_{(102)}^2}{9b_{edge}^2} \quad (2)$$

$$D_{dis} = D_{screw} + D_{edge} \quad (3)$$

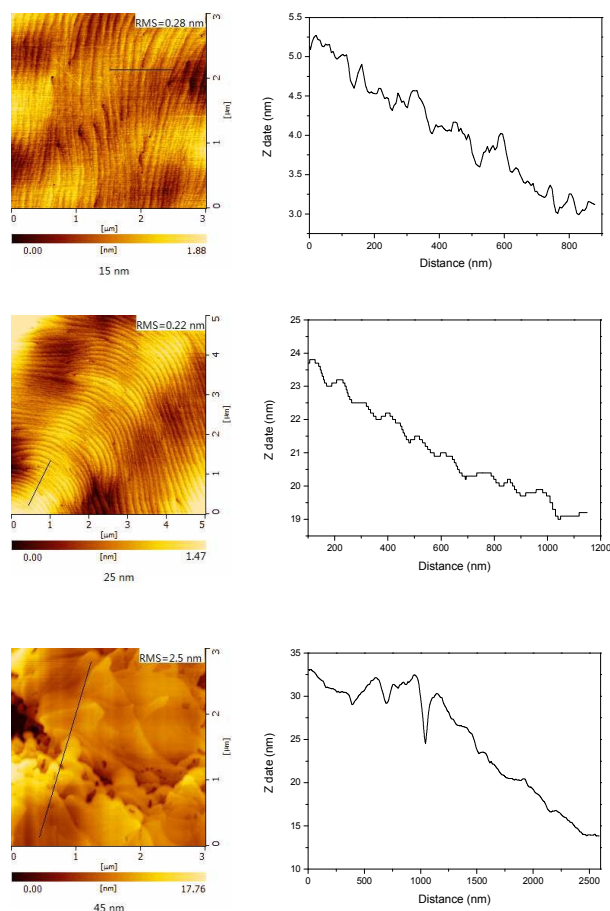


Fig 6 The AFM images (3×3 μm) (left) of bulk GaN with 15, 25 and 45nm-NL thickness and the line profiles of the surface (right).

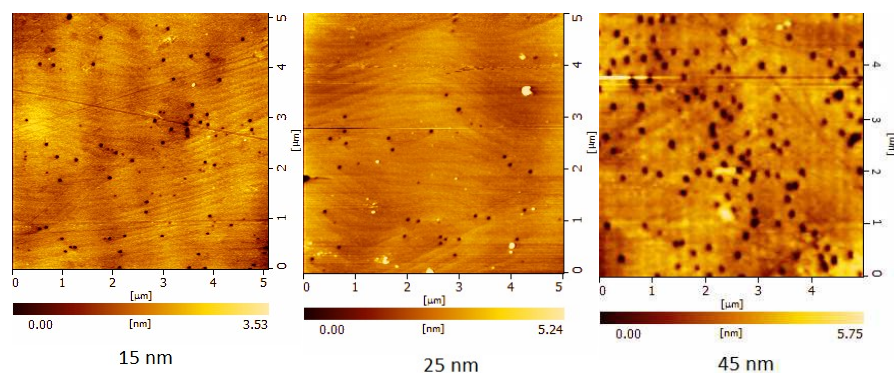


Fig 7 The AFM images ($5 \times 5 \mu\text{m}$) of bulk GaN after etching with 15, 25 and 45nm-NL thickness

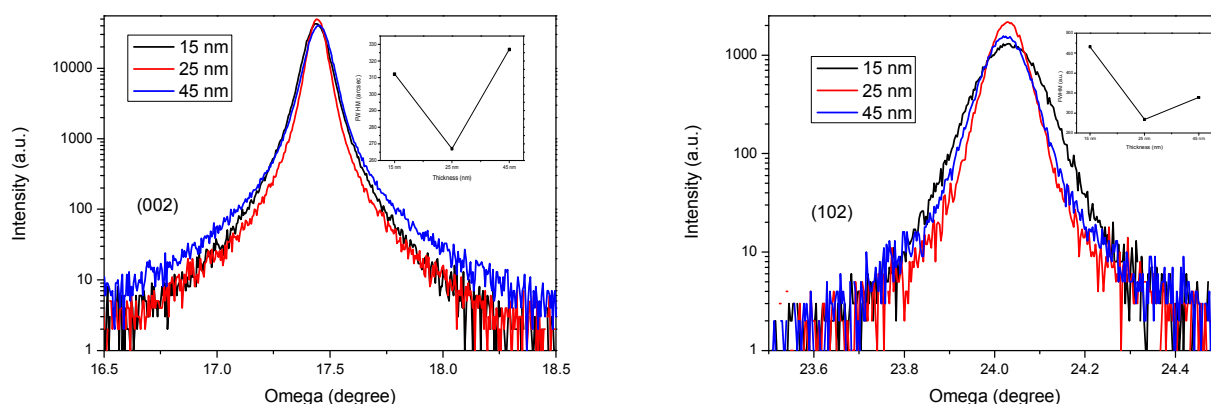


Fig 8 The rocking curve FWHMs of (002) and (102) of bulk GaN with 15, 25 and 45nm-NL thickness

Where D_{screw} is the screw dislocation density, D_{edge} is the edge dislocation density, β is the FWHM values measured for (002) and (102) planes by HRXRD rocking curves and b is the Burgers vector length ($b_{\text{screw}}=0.5185 \text{ nm}$, $b_{\text{edge}}=0.3189 \text{ nm}$), D_{dis} is the total dislocation density. The screw dislocation densities of bulk GaN films with 15, 25 and 45nm-NL thickness are 9.45×10^7 , 6.72×10^7 and $1.04 \times 10^8/\text{cm}^3$, respectively. The edge dislocation densities of bulk GaN films with 15, 25 and 45nm-NL thickness are 5.57×10^8 , 2.06×10^8 and $2.95 \times 10^8/\text{cm}^3$, respectively. The total dislocation densities of the three sample are 6.51×10^8 , 2.73×10^8 and $3.99 \times 10^8/\text{cm}^3$, respectively. The etch pits density is not equal to the XRD measured dislocation density completely which may result from the test point does not origin from the same point of epitaxial wafer. However the tendency which 25 nm-sample has the lowest dislocation density is the same. The smallest FWHM of (002), (102) planes and etch pits density for 25 nm-sample indicate that it has the best crystal quality in the three samples.

Generally, TDs generated at the boundaries of nucleation islands (NIs) are edge-type, and dislocations starting inside the NIs are screw- or mixed-type.²⁹ As stated above, the GaN epilayers are formed by coalescence of the NIs followed by 2D growth process

at high temperature. The NL with fewer grains tends to form larger islands spaced far apart and corresponding 3D growth needs more time. During 3D growth, the NIs grow both vertically and laterally until they coalesce to a continuous film. The screw-type dislocation bends through the lateral growth. When the dislocations meet each other, they are annihilated in the GaN layer by tying up in pairs.³⁰

Based on our experimental results, a schematic of the morphological evolution and associated TD generation and propagation processes discussed above is proposed, as shown in Fig. 9. As for 15nm sample, the NL has the highest density grains before annealing, the NI density is high and the space among them is small after annealing. The spaces between the islands are so small that the lateral growth time required is very short. Thus, the screw-type TDs have less time and chance to bend and terminate, most of them extend to the surface in the following bulk GaN growth process. Meanwhile, many edge-type TDs form at the NIs' boundaries. As the size of grains increases, the film tends to form larger islands with larger space among them. A longer coalescence time for NIs allows more TDs to have chance to bend and annihilate in pairs, thus the quality of GaN epilayer with 25nm-NL gets improved. When the thickness of NL further increases to 45

nm, the height of NIs is not uniform and many small size islands occur after annealing. On the condition that the height of NIs is different, the TDs can not meet each other during NI's coalescence process. In addition, those much smaller NIs increase the boundaries' area where many edge-type dislocations form. Thus the FWHM of (002) and (102) planes increases in this sample.

4. Conclusions

In summary, the NLs' thickness can effectively influence the properties of bulk GaN epilayers and the influence is due to the different NIs' densities and sizes formed during anneal process. As the NL's thickness increases from 15 to 45 nm, the density of

island decreases, accompanied with gradually increasing size, but their uniform becomes worse. The small- and high-density islands corresponding to 15-nm sample tends to grow bulk GaN with numerous edge-type dislocations at the NIs' boundaries. Uniform NIs with larger space corresponding to 25-nm sample can increase the crystal quality. In this case, edge-type dislocations are fewer and screw-type dislocations have more chance to bend and annihilate in the GaN layer by tying up in pairs. However, the nonuniform NIs corresponding to 45-nm sample decreases the interactive probability of bended screw-type dislocations. The redeposited NIs also increases the boundaries' area, more edge-type TDs form at the GaN epilayer. The optimal thickness of the NL to achieve the best crystal quality is 25 nm.

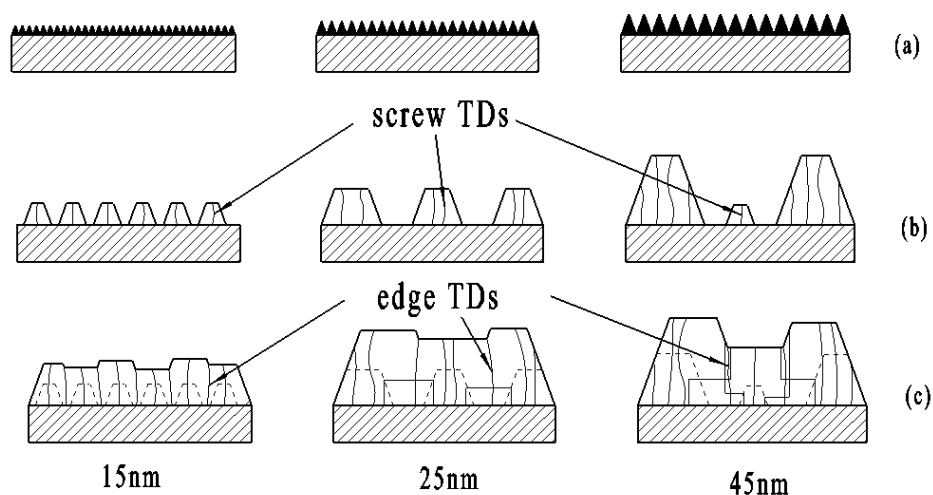


Fig 9 Schematic representation of the morphological evolution and associated dislocation generation and propagation in 15, 25 and 45 nm samples: (a) NIs on sapphire; (b) NIs after annealing; (c) coalescence of NIs with accompanying TDs generation and propagation

Acknowledgements

This work is supported by the National Natural Science Foundation of China (No. 61475110, 61404089 and no. 21471111), the Open Research Fund of Jiangsu Key Laboratory for Solar Cell Materials and Technology, Changzhou University (grant No. 201205), Shanxi Provincial Key Innovative Research Team in Science and Technology (2012041011), the Natural Science Foundation of Shanxi Province (No. 2014021019-1)

References

- S. Nakamura, *J. Crystal Growth*, 1999, **202**, 290.
- R.S. Balmer, C. Pickering, A.M. Kier, J.C.H. Birbeck, M. Saker, T. Martin, *J. Crystal Growth*, 2001, **230**, 361.
- S. J. Rosner, E. C. Carr, M. J. Ludowise, G. Girolami and H. I. Erikson, *Appl. Phys. Lett*, 1997, **70**, 420.
- S. Nakamura, M. Senoh, S. Nagahama, N. Iwasa, T. Yamada, T. Matsushita, Y. Sugimoto and H. Kiyoku, *Jpn. J. Appl. Phys*, 1997, **36**, L1059.
- M.S. Yi, H.H. Lee, D.J. Kim, S.J. Park, D.Y. Noh, C.C. Kim, J.H. Je, *Appl. Phys. Lett*, 1999, **75**, 2187.
- J.N. Kuznia, M. Asif Khan, D.T. Olson, R. Kaplan, J. Freitas, *J. Appl. Phys.* 1993, **73**, 4700.
- L. Sugiura, K. Itaya, J. Nishio, H. Fujimoto, Y. Kokubun, *J. Appl. Phys.*, 1997, **82**, 4877.
- K.S. Kim, C.S. Oh, K.J. Lee, G.M. Yang, C.H. Hong, K.Y. Lim, H.J. Lee, A. Yoshikawa, *J. Appl. Phys.*, 1999, **85**, 8441.
- K. Uchida, A. Watanabe, F. Yano, M. Kouguchi, T. Tanaka and S. Minagawa, *Appl. Phys. Lett*, 1996, **79**, 3487.
- D.J. Kim, Y.T. Moon, K.S. Ahn, S.J. Park, *J. Vac. Sci. Technol. B*, 2000, **181**, 140.
- M. Lunenburger, H. Protzmann, M. Heuken, H. Jurgensen, *Phys. Stat. Sol. A*, 1999, **176**, 727.
- T.B. Ng, J. Han, R.M. Biefeld, M.V. Weckwerth, *J. Electron. Mater.*, 1998, **274**, 190.
- M. Siegert and M. Plischke, *Phys. Rev. Lett*, 1994, **73**, 1517.
- F. Ruffino, V. Torrisi, G. Marletta and M.G. Grimaldi, *Applied Physics A*, 2010, **100**, 7.
- F. Ruffino and M. G. Grimaldi, *J. Appl. Phys*, 2010, **107**, 104321.
- M. Lada, A.G. Cullis, P.J. Parbrook, *J. Crystal Growth*, 2003, **258**, 89.
- K. Lorenz, M. Gonsalves, W. Kim, V. Narayanan, S. Mahajan, *Appl. Phys. Lett*. 2000, **77**, 3391.

- 18 V. Narayanan, K. Lorenz, W. Kim, S. Mahajan, *Philos. Mag. A* 2002, **82**, 885.
- 19 C. V. Thompson, *J. Appl. Phys.*, 1985, **58**, 763.
- 20 C. V. Thompson, H. J. Frost and F. Spaepen, *Acta Metall.*, 1987, **35**, 887.
- 21 F. Ruffino, M.G. Grimaldi, C. Bongiorno, F. Giannazzo, F. Roccaforte, V. Raineri and C. Spinella, *J. Appl. Phys.*, 2009, **105**, 054311.
- 22 X. H. Wu, P. Fini, E. J. Tarsa, B. Heying, S. Keller, U. K. Mishra, S. P. DenBaars and J. S. Speck, *J. Cryst. Growth*, 1998, **231**, 189.
- 23 Shuti Li, Jun Su, Guanghan Fan, Yong Zhang, Shuwen Zheng, Huiqing Sun, Jianxing Cao, *J. Crystal Growth*, 2008, **310**, 3722.
- 24 R. Chierchia, T. Böttcher, H. Heinke, S. Einfeldt, S. Figge, and D. Hommel, *J. Appl. Phys.*, 2003, **93**, 8918.
- 25 H. Heinke, V. Kirchner, S. Einfeldt, and D. Hommel, *Appl. Phys. Lett.*, 2000, **77**, 2145.
- 26 M.E. Vickers, M.J. Kappers, R. Datta, C. McAleese, T.M. Smeeton, F.D. G. Rayment, and C.J. Humphreys, *J. Phys. D.*, 2005, **38**, A99.
- 27 P. Gay, P.B. Hirsch, and A. Kelly, *Acta Metall.*, 1953, **1**, 315.
- 28 S. S. Kushvaha, M. Senthil Kumar, K. K. Maurya, M. K. Dalai, and Nita D. Sharma, *AIP ADVANCES*, 2013, **3**, 092109.
- 29 X.J. Ning, F.R. Chien, P. Pirouz, J.W. Yang, M.A. Khan, *J. Mater. Res.*, 1996, **11**, 580.
- 30 X. Weng, S. Raghavan, J.D. Acord, A. Jain, E.C. Dickey, J.M. Redwing, *J. Crystal Growth*, 2007, **300**, 217.